



# Structure Design and Optimization of the Mass Flow Distribution Device of Downcomer for Fluoride-Salt-Cooled High-Temperature Advanced Reactor – FuSTAR

Xinyu Li, Dalin Zhang<sup>(✉)</sup>, Xingguang Zhou, Wenxi Tian, and Suizheng Qiu

Xi'an Jiaotong University, Xi'an, Shaanxi, China  
dlzhang@mail.xjtu.edu.cn

**Abstract.** The new generation of water-free cooling reactors: the FuSTAR system (Fluoride-Salt-cooled high-Temperature Advanced Reactor), mainly proposed by Xi'an Jiaotong University, is at the design stage. So far, the overall parameters of the heat transport system of FuSTAR have been obtained, and there is a pressing need to design and optimize the mass flow distribution device of Downcomer. In this paper, to obtain the specific parameters of structure matching the design values of mass flow rate, the finite element analysis was adopted, combined with the Nelder-Mead algorithm in the nonlinear programming. The results show that the mass flow distribution device with a multiple-port plate structure can achieve the purpose of the values of mass flow rate. Moreover, the mass flow rate is not so sensitive to the geometric parameters of these structures, which means more engineering margin. Based on this research, the detailed structural parameters and physical information about the distribution device were obtained, and the data from numerical tests can be used to build the proxy models to speed up transient analysis programs of FuSTAR.

**Keywords:** Mass Flow · Distribution · Downcomer · FuSTAR · Finite Element Analysis

## 1 Introduction

Small Modular Fluoride salt-cooled High-temperature Reactor (SMFHR) equipped with solid fuel and liquid-salt coolant, has the advantages of inherent safety, compact structure, high temperature, and modularity, which can be built in remote areas and inland water shortage, underground mines, industrial park facilities, military bases, etc., to provide the solutions of multi-purpose integrated energy [1]. Fluoride-Salt-cooled high-Temperature Advanced Reactor (FuSTAR) is a new generation of water-free reactor technology proposed by Xi'an Jiaotong University, which uses the integrated SMFHR as the heat source, modular molten salt pool as the energy storage device, and closed Brayton power cycle as energy conversion system. At present, the design of the core neutronics-thermohydraulics-power cycle system has been completed, and a safety analysis is needed to verify the inherent safety. The integrated structure is adopted in FuSTAR

and shown in Fig. 1. The coolant is FLiBe salt, which is heated from the core and enters the riser, then flows down into the Primary Heat Exchanger (PHE) to release the heat. The Cold salt is then pressured by the pump and split into two paths: one is along the Downcomer and returns into the core, and the other flow across the Downcomer and flows up into the Direct heat Exchanger (DHE) to constitute the steady loop of Passive Residual Heat Removal System (PRHRS).

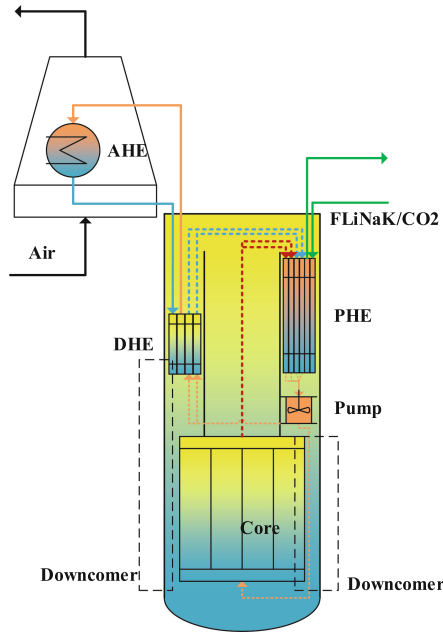


Fig. 1. Integrated interior structure of FuSTAR

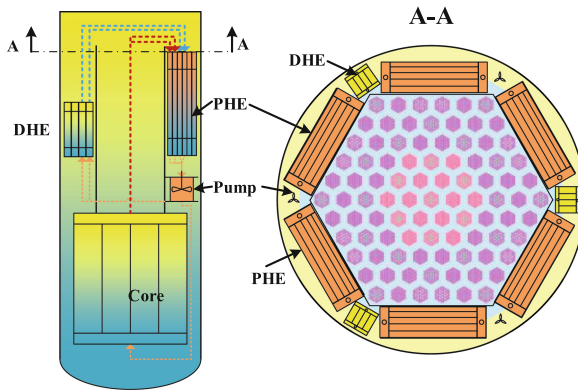


Fig. 2. Cross-section of heat exchangers and reactor

Figure 2 shows the layout scheme of the heat exchangers and reactor, with a total of 6 PHEs and 3 DHEs installed alternately around the riser. After neutronics and burnup calculations [2], the decay heat accounts for 1% of the total power thermal heat from the core, which must be removed by three DHEs of PRHRS.

However, the structure mentioned above has an obvious backflow region of Downcomer, which is difficult to be described by one-dimensional thermal-hydraulics equations. Therefore, detailed structural design and analysis are required. In this paper, the computational fluid dynamics method (CFD) is used to design the detailed structure of the Downcomer to ensure the flow distribution is as same as that of the design value. At the same time, the results of flow distribution are less sensitive to the structure, which is feasible in engineering processing. In addition, the numerical results or experimental results of the structure can provide equivalent resistance coefficients for the one-dimensional thermal-hydraulics and safety analysis programs.

## 2 Methodologies

### 2.1 Thermodynamic and Geometry Boundaries

The flow distribution and thermodynamic boundary were calculated by the energy balance method, and the thermophysical properties were referred to TRACE and CoolProp [3, 4]. 1/6 axisymmetric initial geometric structure was used for modeling, and Fig. 3 shows the boundary conditions and complete structure of the fluid domain with streamlines. The uniform velocity at the inlet boundary, the zero gradient outlet boundary at the outlet to DHEs, and the zero gauge pressure at the bottom annular outlet were used.

### 2.2 Design and Optimization Method

In this paper, the processes of design and optimization are shown in Fig. 4, which are mainly divided into two parts: preliminary analysis and secondary analysis. The Finite Element Method (FEM) was used to discretize space [5] based on COMSOL software.

In the preliminary analysis, to realize automation, the grid sequence should be established first for automatic generation. Subsequently, the robust and simple turbulence model was used to directly calculate the flow distribution and the optimization algorithms are adopted to change the structural parameters, minimizing the deviation between the calculated flow distribution and the design value. The sensitivity of structural parameters was analyzed based on the optimal solution to check if there are parameters that significantly affect the distribution. If the structure sensitivities are too strong, the structure needs to be changed and re-analyzed.

In the secondary analysis, suitable turbulence models for specific structures were selected, and optimization and sensitivity analyses were performed again for the optimal structures in the preliminary analysis. To ensure accuracy, the second-order element is used in the optimization stage. While to ensure efficiency, the first-order element is used in the sensitivity analysis stage.

The standard  $k-\varepsilon$  turbulence model was used in the preliminary analysis because of its robustness [6]. In the secondary analysis, as there are phenomenons of boundary layer

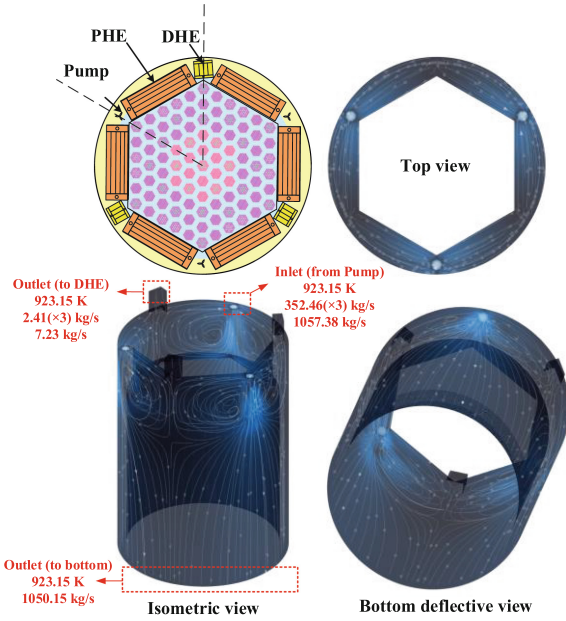


**Fig. 3.** Boundary conditions and complete structure of the fluid domain with streamlines.

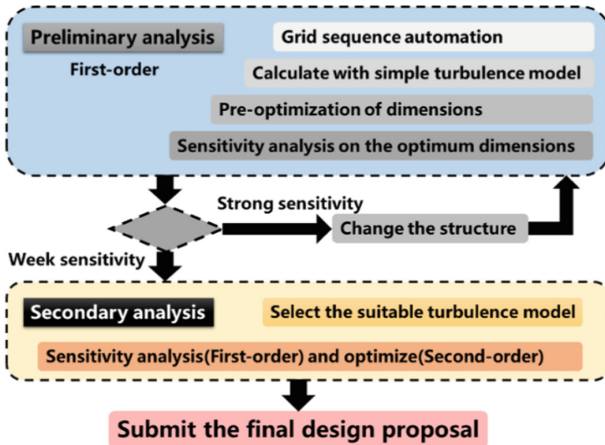


**Fig. 4.** The processes of design and optimization on Downcomer

separation and mainstream impact on the wall in the geometric structure in Fig. 3, the Spalart-Allmaras model with the anisotropic transport effect of turbulent viscosity [7], and the v2f model with the anisotropy of pulsation velocity [8], both of which have been applied.

In the solving process, the linear equations are calculated by PARDISO direct solver [9], the nonlinear part is separated and iterated by the Newton method, and the original

variables of the NS equation and turbulent variables are calculated successively. In the process of optimization, the Nelder-Mead algorithm was adopted [10]. The decision variables are the dimensions of the structure, and the objective function is the deviation between the calculated value and the designed value of flow distribution. When the deviation is zero, the optimization is completed.

### 3 Results and Discussion

#### 3.1 Preliminary Analysis

The parameters initially involved in the optimization calculation are inlet-diameter and riser-height. After 37 times of optimization calculations, the final dimensions and velocity field are shown in Fig. 5, where the flow deviation at the outlet to DHE is only 0.09 kg/s. It is obvious that once the fluid enters the Downcomer, it will undergo sudden separation, accompanied by a large adverse pressure gradient. Subsequently, part of the large vortex impacts the riser region at the bottom, introducing pulsating velocity anisotropy. Then in the ring section, the vortex and mass flow rate separate. One-dimensional and two-dimensional safety analysis programs cannot capture this process, so they need to be developed again and introduce empirical relations.

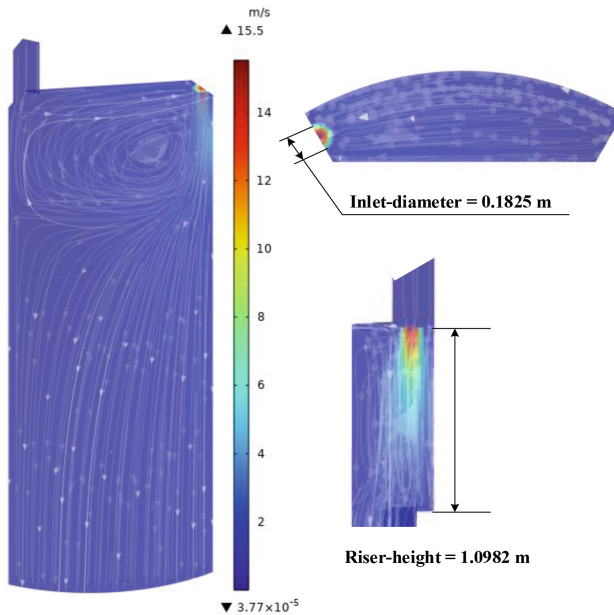
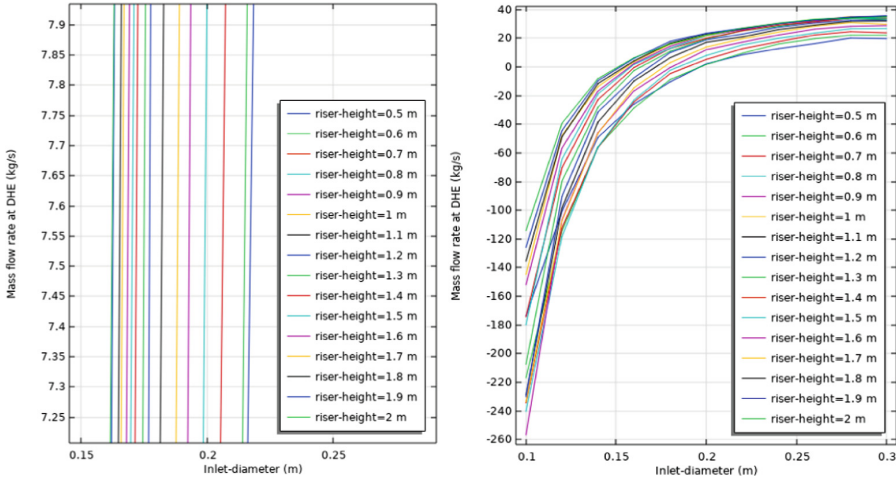


Fig. 5. Optimal dimensions and velocity in preliminary analysis

Based on the preliminary optimal dimensions above, dimension sensitivity analysis is carried out to judge the feasibility of the structure in engineering.

The influence on the mass flow rate of DHE by inlet-diameter under different riser-heights is shown in Fig. 6. The inlet-diameter has a great influence on the mass flow rate of DHE. For every 1 mm increase in inlet-diameter, the flow rate increases by 1 kg/s, which is difficult to control in engineering because the rated mass flow rate of DHE is only 7.23 kg/s.



**Fig. 6.** The influence on the mass flow rate of DHE by inlet-diameter

The influence on the mass flow rate of DHE by riser-height under different inlet-diameters shown in Fig. 7. The sensitivities on riser-height are really weak, so the machining accuracy of riser-height can be appropriately relaxed in engineering.

To sum up, the flow distribution ratio of DHE in the preliminary structure is greatly affected by the inlet-diameter, which is unstable to rely on a split of the large vortex. Therefore, it is necessary to improve the geometry structure to weaken the sensitivities of dimensions. In addition, the stability in the calculation process is very well, so the Spalart-Allmaras model was used later to better describe the boundary layer and anisotropic effect. Finally, the optimal scheme is calculated and compared with the  $v2f$  model.

### 3.2 Sensitivity Weakening and Structural Optimization

The improved structure design is shown in Fig. 8. Relying only on a large vortex for flow distribution would be difficult to control, so consider a separator plate in the vortex area on the riser. The plate divides the upstream fluid into two parts, one flowing laterally to the outlet at the DHE, and the other flowing downstream to the bottom of the Downcomer. In addition, to better control the outlet flow at the DHE, this outlet is also assembled in a single hole plate, through the size of the hole to obtain a different flow distribution. Therefore, the structural variables are updated as new decision variables in optimization, which are: **split-height**, **Theta**, **inlet-diameter**, **Outlet-diameter**, and **riser-height**.

**Split-height** represents the distance between the separator plate and the top, of which range is constrained as 0.05–0.15m. The initial value is 0.06 m.

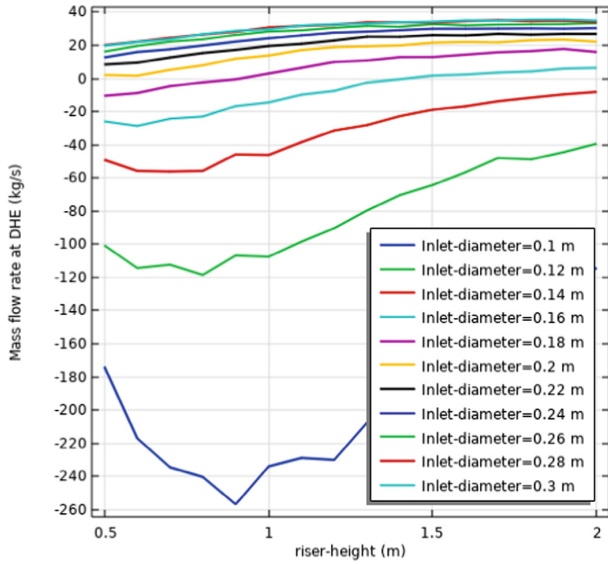


Fig. 7. The influence on the mass flow rate of DHE by riser-height

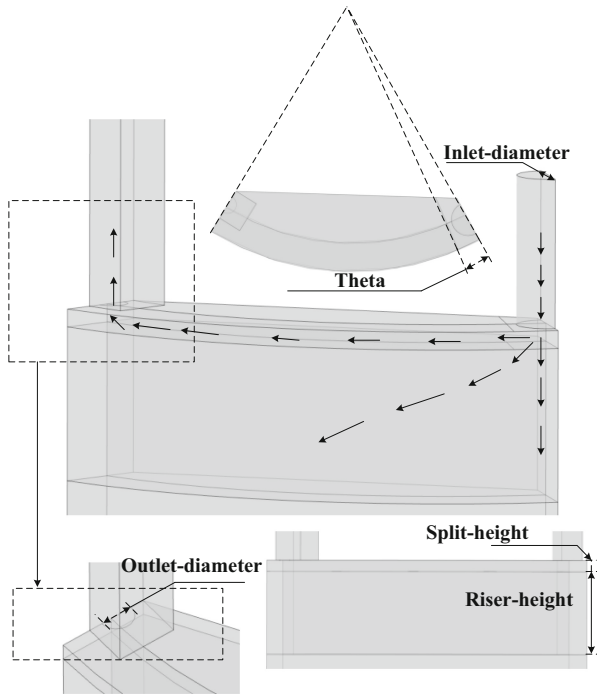


Fig. 8. Improved structure design and updated new decision variables

Theta represents the opening angle of the separator plate, which is calibrated based on the central axis of the reactor and its variation range is constrained as  $5\text{--}50^\circ$ . The initial value is  $5^\circ$ .

**Inlet-diameter** still represents the diameter at the inlet, upstream of which is the fluid at the pump outlet. Due to the constrained size of the container, its range is limited to  $0.1\text{--}0.25$  m. The initial value is  $0.21$  m.

**Outlet-diameter** represents the hole diameter of the hole plate at the outlet, and its downstream is the entrance of the DHE. Limited by the size of the outlet channel, its range is limited to  $0.05\text{--}0.15$  m. The initial value is  $0.11$  m.

**Riser-height** still represents the height of the riser in the flow domain, which does not include the split-height. The range of riser-height is constrained to  $0.2\text{--}2$  m. The initial value is  $0.5$  m.

Considering the more complex structures, the separation and attachment of boundary layer become more complicated, so the Spalart-Allmaras model was used for calculation. For the final scheme, the  $\nu 2f$  model was also used to compare.

### Stepwise Sensitivity Analysis and Selection of Stability Region

The stepwise sensitivity analysis parameters were scanned to find the stability region of each parameter. To save time on calculation, the first-order element was used to discretize the space. The higher-order elements only have some quantitative differences compared to the first-order element, but do not affect the qualitative results of sensitivity analysis.

First, the sensitivities of the split-height and the theta on the flow distribution ratio of DHE in their range were analyzed when other parameters were set to their initial values, as shown in Fig. 9. With the increase of the theta and the split-height, the mass flow rate increases gradually but the slope decreases. The stable slope can be controlled well only when both the theta and the split-height are small. Therefore, the theta =  $5^\circ$  and the split-height =  $0.06$  m are selected within the stable ranges of low slope. The structural sensitivities decreased from  $1(\text{mm}/(\text{kg}/\text{s}))$  to about  $4(\text{mm}/(\text{kg}/\text{s}))$ , split-height) and  $60(\text{mm}/(\text{kg}/\text{s}))$ , theta), which are  $1/4$  and  $1/60$  of the original.

Then, based on the above parameters selected, the sensitivities analysis of the inlet-diameter and the outlet-diameter on the flow distribution ratio of DHE were carried out. The analysis results are shown in Fig. 10. When the inlet-diameter is about  $0.2$  m and the outlet-diameter is about  $0.1$  m, the slope is the lowest with weak sensitivity. Therefore, the inlet-diameter =  $0.21$  m and the outlet-diameter =  $0.11$  m. The structural sensitivities decreased from  $1(\text{mm}/(\text{kg}/\text{s}))$  to about  $13(\text{mm}/(\text{kg}/\text{s}))$ , inlet-diameter) and  $15(\text{mm}/(\text{kg}/\text{s}))$ , outlet-diameter), which are  $1/13$  and  $1/15$  of the original.

Finally, the above parameters were fixed and the sensitivity analysis of the riser-height on the flow distribution ratio of DHE was conducted. The results are shown in Fig. 11. The mass flow rate is not affected significantly by the riser-height. Therefore, the values in all the range of riser-height can be used. The structural sensitivity decreased from  $1(\text{mm}/(\text{kg}/\text{s}))$  to about  $800(\text{mm}/(\text{kg}/\text{s}))$ , which is  $1/800$  of the original.

### Structural Optimization in the Stability Region

Structural parameters optimization was carried out based on the stability region above. To ensure accuracy, the second-order element was used to discretize the space. The riser-height has the lowest sensitivity to mass flow rate, so only it was used as the decision



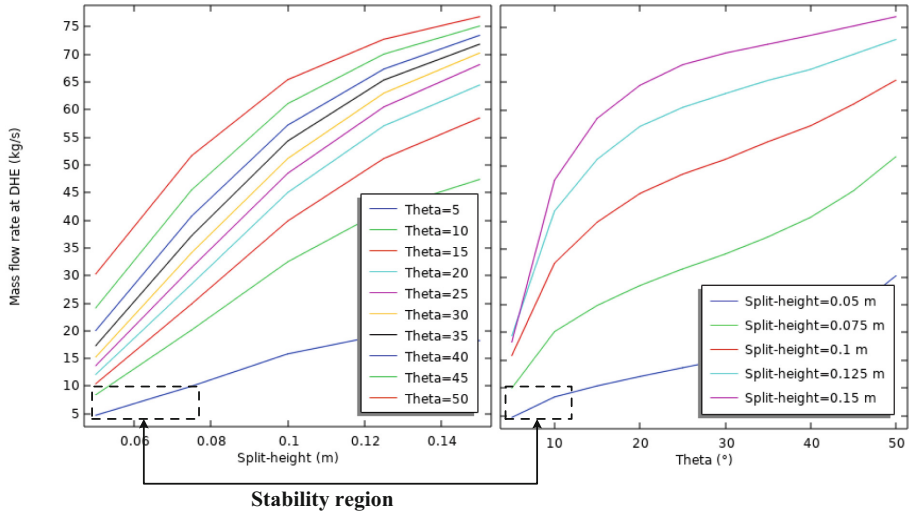


Fig. 9. The sensitivities of split-height and theta

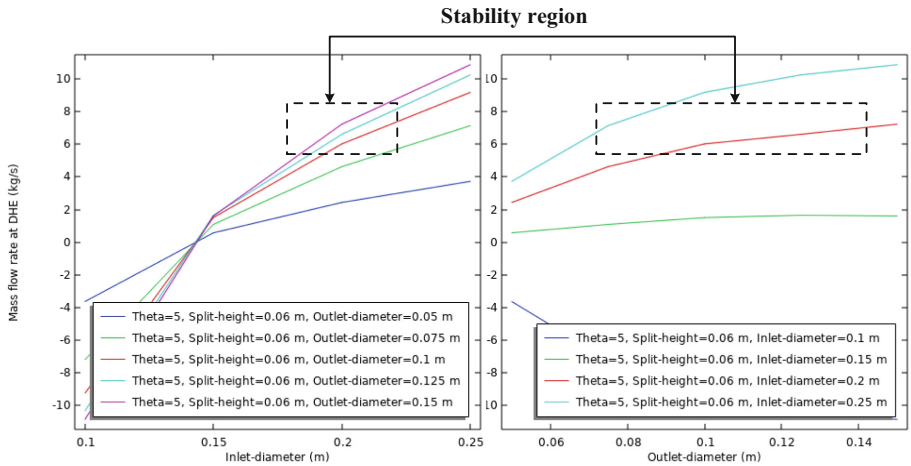


Fig. 10. The sensitivities of inlet-diameter and outlet-diameter

variable, and other variables are not optimized to avoid shifting out of the stability domain. The objective function is the deviation of the outlet mass flow rate at the DHE from the design value – 7.23 kg/s. The Nelder-Mead algorithm was selected and the process of optimization is shown in Fig. 12. Finally, the value of riser-height stabilized at 1.3375 m, where the deviation between the calculated mass flow rate and the designed value was minimum to zero, and the optimization was completed.

The distribution of  $y^+$  and the global velocity field of the optimal solution are shown in Fig. 13. The global maximum value of  $y^+$  is 3.76 at the inlet due to the uniform boundary of velocity, while it of other parts is about 1, which meets the requirements

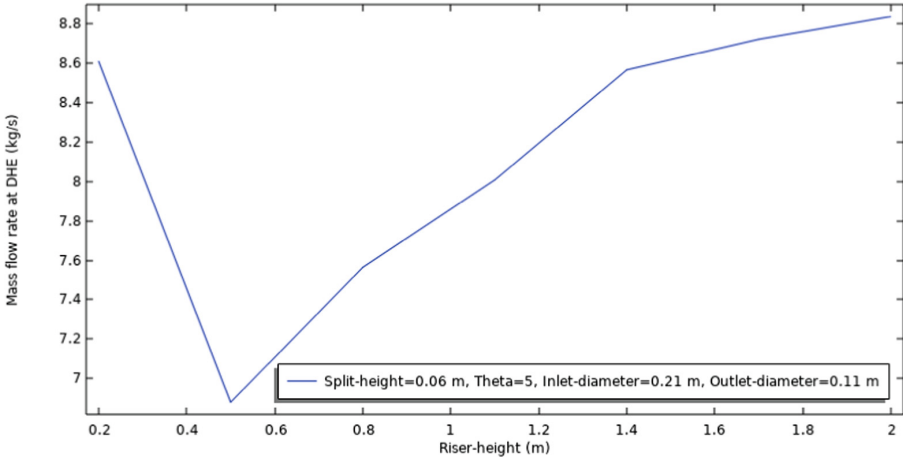


Fig. 11. The sensitivities of riser-height

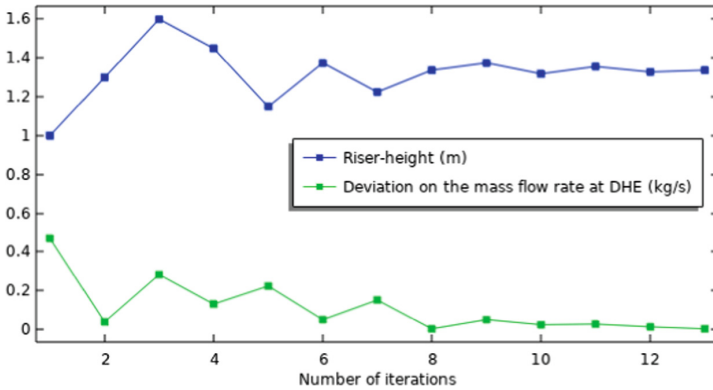
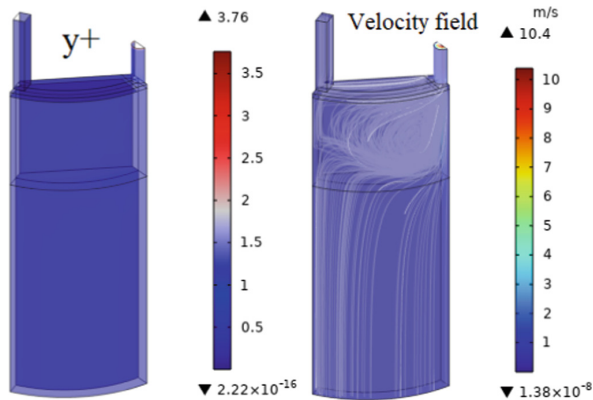


Fig. 12. Optimization of the riser-height with minimal deviation

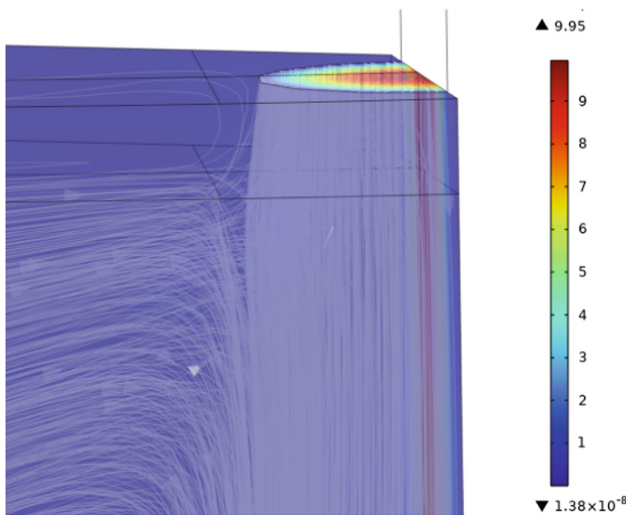
of boundary layer analysis of the Spalart-Allmaras model. According to the streamline, most of the flow forms a stagnant vortex in the riser region, and a small part of the fluid flows horizontally along with the separator plate to the outlet at DHE. As can be seen from the sensitivity analysis above, this structure of flow separation has low geometric sensitivity and is suitable for engineering processing (Fig. 14).

Figure 15 shows the velocity field at the longitudinal section of the inlet. With the riser-height of 1.3375 m, the mainstream flow velocity at the riser bottom has attenuated from 10 m/s to 4 m/s, which weakens the anisotropic impact effect and is also an important reason why the wall  $y^+$  always keeps a low level. Lower impact momentum results in less vibration and direct pressure, which also improves the long-term operating life of the structure.

Figure 16 shows the velocity field of the outlet at DHE and the mesh diagram. The second-order element only needs the thicker mesh to be able to resolve the streamline of



**Fig. 13.** The  $y^+$  and global velocity field of the optimal solution



**Fig. 14.** Velocity field and streamline at the inlet of the separator plate

the curve well. By changing the diameter of the hole plate, the sensitivity of the structure is lower, which is about 15 times that of the original scheme, and is more beneficial to engineering processing.

Finally, the  $v2f$  model with the same parameters was used to verify the results of the Spalart-Allmaras model. The comparison of overall results is shown in Table 1. The results show that the error of the Spalart-Allmaras model and  $v2f$  model is really small, the maximum error of pressure drop is less than 1.5%, and that of the mass flow rate is at the magnitude of  $10^{-5}$ . Therefore, to get the macro parameter of mass flow rate and pressure drop, the Spalart-Allmaras model with faster speed and stronger stability can be considered in the design work. The final dimensions based on Fig. 8 are summarized in Table 2.

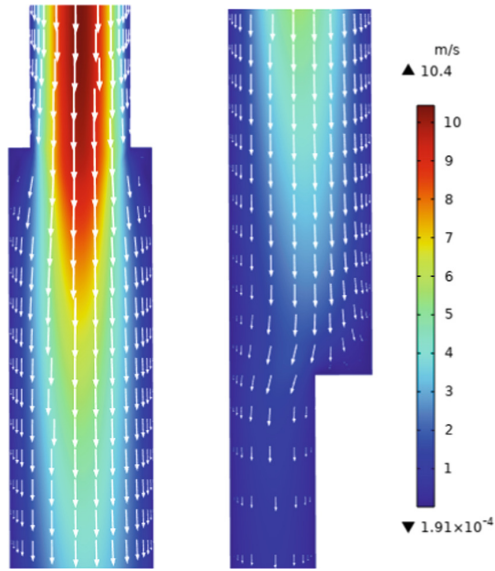


**Fig. 15.** Velocity field at the longitudinal section of the inlet (The top of the right image continues at the bottom of the left)

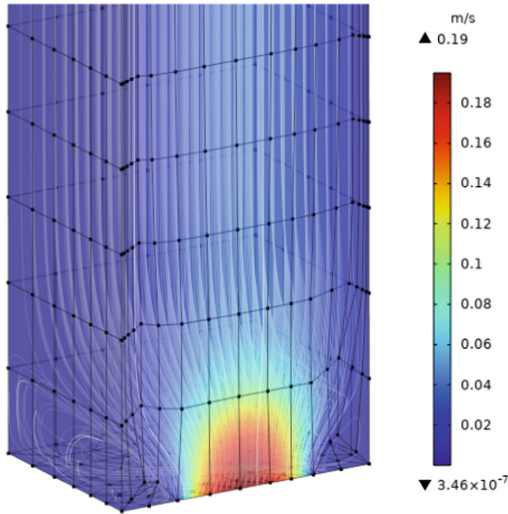


**Fig. 16.** Velocity field of the outlet at DHE and the mesh diagram

**Table 1.** Comparison of overall results with Spalart-Allmaras and  $\nu 2f$  turbulence model

| <b>Turbulence model</b>                         | <b>Spalart – Allmaras</b> | <b><math>\nu 2f</math></b> | <b>Deviation(based on <math>\nu 2f</math>)</b> |
|---|---------------------------|----------------------------|--|
| Mass flow rate at bottom of Downcomer           | 1050.14648 kg/s           | 1050.14598 kg/s            | 4.76E-07                                       |
| Pressure drop from inlet to bottom of Downcomer | 10651.14 Pa               | 10522.64 Pa                | 1.22%  |
| Mass flow rate of outlet at DHE                 | 7.2435 kg/s               | 7.2440 kg/s                | -6.90E-05                                      |
| Pressure drop from inlet to outlet at DHE       | 92066.58 Pa               | 92195.09 Pa                | -0.14%   |

**Table 2.** The final dimensions based on Fig. 8

| <b>Parameters</b> | <b>Values</b> | <b>Units</b> |
|-------------------|---------------|--------------|
| Split-height      | 60            | mm           |
| Theta             | 5             | °            |
| Inlet-diameter    | 210           | mm           |
| Outlet-diameter   | 110           | mm           |
| Riser-height      | 1.3375        | m            |

## 4 Conclusions

In this paper, the CFD method was used to design the detailed structure of the Downcomer to ensure the flow distribution is as same as that of the design value. 1/6 axisymmetric initial geometric structure was used for modeling, and the processes of design and optimization are divided into two parts: preliminary analysis and secondary analysis. The standard k- $\epsilon$  model, Spalart-Allmaras model, and  $\nu 2f$  model were used and compared respectively, and the Nelder-Mead algorithm was used for the optimization.

The results of the preliminary analysis showed that in the ring section, the vortex and mass flow rate separate. One-dimensional and two-dimensional safety analysis programs cannot capture this process, so they need to be developed again and introduce empirical relations. However, the flow distribution ratio of DHE in the preliminary structure is greatly affected by the inlet-diameter, which is unstable to rely on a split of the large vortex.

The results of the secondary analysis showed a hole plate at the outlet and a separator plate in the vortex area on the riser will reduce structural sensitivity by 1/4 to 1/800. Most of the flow forms a stagnant vortex in the riser region, and a small part of the fluid flows horizontally along with the separator plate to the outlet at DHE. Lower impact momentum at the bottom of the riser results in less vibration and direct pressure, which also improves the long-term operating life of the structure. Finally, the results show

that the error of the Spalart-Allmaras model and v2f model is really small. The Spalart-Allmaras model with faster speed and stronger stability can be considered in the design work.

**Acknowledgement.** This research is supported by the National Key Research and Development Program of China (Grant No. 2020YFB1902000).

## References

1. Jiang, D., et al.: Fluoride-salt-cooled high-temperature reactors: review of historical milestones, research status, challenges, and outlook. *Renew. Sustain. Energy Rev.* **161**, 112345 (2022). <https://doi.org/10.1016/j.rser.2022.112345>
2. Zhou, X., et al.: A coupling analysis method of the thermal hydraulics and neutronics based on inverse distance weighted method, p. 12
3. Bell, I.H., Wronski, J., Quoilin, S., Lemort, V.: Pure and pseudo-pure fluid thermophysical property evaluation and the open-source thermophysical property library CoolProp. *Ind. Eng. Chem. Res.* **53**(6), 2498–2508 (2014). <https://doi.org/10.1021/ie4033999>
4. Richard, J., et al.: Implementation of liquid salt working fluids into TRACE, p. 11 (2014)
5. Hughes, T.J.R., Mallet, M.: A new finite element formulation for computational fluid dynamics: III. The generalized streamline operator for multidimensional advective-diffusive systems. *Comput. Meth. Appl. Mech. Eng.* **58**(3), 305–328 (1986). [https://doi.org/10.1016/0045-7825\(86\)90152-0](https://doi.org/10.1016/0045-7825(86)90152-0)
6. Wilcox, D.: *Turbulence Modeling for CFD*, 3rd edn. (Hardcover) (2006)
7. Dacles-Mariani, J., Bradshaw, P., Chow, J.S., Zilliac, G.: Numerical/experimental study of a Wingtip Vortex in the near field. *AIAA J.* **33**, 1561–1568 (2012)
8. Laurence, D., Uribe, J., Utyuzhnikov, S.: A robust formulation of the v2-f model. *Flow Turbul. Combust.* **73**, 169–185 (2005). <https://doi.org/10.1007/s10494-005-1974-8>
9. Alappat, C., et al.: A recursive algebraic coloring technique for hardware-efficient symmetric sparse matrix-vector multiplication. *ACM Trans. Parallel Comput.* **7**(3), 1–37 (2020). <https://doi.org/10.1145/3399732>
10. Conn, A.R., Scheinberg, K., Vicente, L.N.: *Introduction to derivative-free optimization*. Society for Industrial and Applied Mathematics/Mathematical Programming Society, Philadelphia (2009)

**Open Access** This chapter is licensed under the terms of the Creative Commons Attribution 4.0 International License (<http://creativecommons.org/licenses/by/4.0/>), which permits use, sharing, adaptation, distribution and reproduction in any medium or format, as long as you give appropriate credit to the original author(s) and the source, provide a link to the Creative Commons license and indicate if changes were made.

The images or other third party material in this chapter are included in the chapter's Creative Commons license, unless indicated otherwise in a credit line to the material. If material is not included in the chapter's Creative Commons license and your intended use is not permitted by statutory regulation or exceeds the permitted use, you will need to obtain permission directly from the copyright holder.

